Analysing the Performance of Incremental Quantity based Directional Time-Domain Protection near HVAC Cables and VSC HVDC Converters

J. Vermunicht, W. Leterme, D. Van Hertem

***Abstract*—New grid elements such as Voltage Source Converters (VSC) and cables are being increasingly used in today's power grid. These new grid elements behave differently compared to synchronous machines and overhead lines during transients and faults, impacting the present system's legacy protection. An increased share of underground cables affects the system's resonance frequencies whereas VSCs introduce actively controlled current phase shifts during short-circuit faults. Existing research mainly focuses on VSC impacts on phasor-based legacy protection. This paper studies the impact of these new grid elements on incremental quantity-based directional protection, which operates in the time domain, using EMT-type models and hardware experiments. First, cables introduce low frequency oscillations for remote, single phase faults and additionally under weak grid conditions. At low frequencies, these oscillations are not filtered out by the protection, which may result in a decrease of dependability margin (23% of the tested cases) and potential security issues. For the majority of studied cases, the relays worked correctly. Second, fast reactive current injection by a VSC can cause malfunction of incremental quantity protection. Malfunction occurred in 1 case and a decrease of dependability in 10% of the tested cases. This is especially problematic for grids with relatively low synchronous infeed.**

***Keywords*—Cable transient, Directional protection, Incremental quantities, Time-domain algorithms, Transmission line protection, VSC**

I. Introduction

NEW grid elements such as High Voltage Direct Current (HVDC) interconnections, Voltage Source Converters (VSC) and underground cables at transmission level are being deployed to facilitate the expansion of renewable energy sources and future demand of electric power. These new grid elements behave different compared to synchronous machines and overhead lines during transients and faults, impacting legacy protection in the present AC system. An increasing amount of cables in the system decreases the system's resonance frequencies [1]. Cable induced oscillations are superimposed on the currents and voltages when triggered by switching events or faults. Regarding inverter-based grid elements, VSC controls introduce phase angle shifts during faults. These phase shifts depend on the converter control and fault-ride-through strategy [2].

This work is part of the Neptune project, supported by the Energy Transition Fund, FOD Economy, Belgium. The authors are with the Dept. Electrical Engineering, KU Leuven/EnergyVille, Leuven/Genk, Belgium (e-mail: joachim.vermunicht@esat.kuleuven.be).

Paper submitted to the International Conference on Power Systems Transients (IPST2023) in Thessaloniki, Greece, June 12-15, 2023.

Various time-domain protection algorithms are described in the literature, and can be categorised under traveling wave (TW) and incremental quantity (IQ) algorithms, also referred to as superimposed quantity or delta quantity [3]–[5]. One of the features of time-domain algorithms is the increase in speed compared to phasor-based approaches [6]–[8]. Time-domain algorithms are applied in commercially available protection devices, for example for IQ-based directional protection in [4], [9], IQ-based distance and TW-based protection in [9]. For decades, IQ algorithms are applied in parallel with phasor-based algorithms for example in [4]. Individual time-domain algorithms are successfully tested on real-world fault records and for double circuit lines [10], [11]. Moreover, near unconventional sources, time-domain algorithms are being proposed as part of the solution for example for directional supervision [12].

However, near converter interfaced sources, few studies indicate problems with IQ-based protection due to a negative impact on the magnitude and angle of the incremental current [13], [14]. Although many recent studies have analysed problematic VSC interactions with conventional phasor-based protection such as distance protection e.g. in [15]–[20], few studies focus on how IQ-based transmission line protection performs under changed source conditions e.g. in the vicinity of underground cables or VSCs. Therefore, it remains unclear whether IQ algorithms could be a full replacement for phasor-based protection and what the attention points are.

While conventional protection filters and only acts on the fundamental (50 Hz) frequency component, time-domain protection processes all transient information within a certain frequency range. The bandwidth of the input filter thus increases for time-domain protection. As a consequence, time-domain algorithms may also process the cable induced oscillations and phase shifts originating from VSC control during faults. IQ-based techniques analyse basically the fundamental component, although without filtering that fundamental component as a phasor. For IQ algorithms this could cause malfunction as previously described phenomena are not filtered out.

This study analyses the impact of changing infeed conditions by new grid elements on IQ-based directional line protection. The aim of this study is twofold: analysing the impact of (i) cable induced oscillations and (ii) changed injection angles by VSCs during faults on the dependability of incremental quantity-based directional protection.

II. Background and models

This section starts with a summary of IQ for protection and next introduces the VSC model used for this study.

A. Incremental quantity protection

Incremental quantities (IQs), also called superimposed or delta components, are difference components. When a fault or other transient occurs, the system's currents and voltages differ from the pre-fault quantities. This difference component constitutes the IQs [3]:

$$\Delta i = i(t) - i(t - pT) \tag{1}$$

with Δi the incremental current, $i(t)$ the measured instantaneous current and $i(t - pT)$ the current measured an integer number (p) of fundamental cycles earlier. The same applies to the incremental voltage.

The main advantage of using IQs is the separation from the pre-fault power flow, IQs thus depend only on the faulted network itself and the fault incident angle [3], [5]. However, this is only valid as long as the IQs originate from one unique and passive fault source. The IQs in most existing applications assume network elements based on constant and lumped impedances (resistors and inductors).

B. VSC model with variable post-fault time stages

The converter is represented by an averaged model with voltage source and equivalent impedance per phase. The controls include inner current controls in a static dq-frame using a phase-locked loop (PLL) and outer controls for active and reactive power similar as in [21], [22]. The model implemented for this work allows to study symmetric faults as it controls only the positive sequence, which suffices for the scope of this study. The fault-ride-through (FRT) control strategy (Fig. 1) is voltage support, and becomes active when the voltage at the coupling point drops below 80%. During voltage support, positive sequence reactive current is injected and prioritised over active current. This fast fault current injection corresponds with for example German grid code implementation [22].

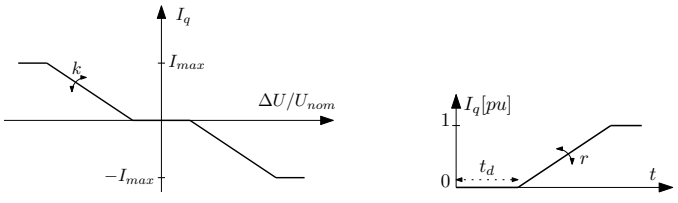

(a) ΔI_q-injection (b) Time variation

Fig. 1: The VSC fast fault current injection during FRT can be controlled in this model by three parameters. The magnitude of reactive current injection is a function of the voltage drop and injection parameter *k*. The time delay t_d before injection and ramp rate *r* determine the time variation of the reactive current injection.

The generic VSC model with grid following controls developed for this study allows control of VSC dynamics during two different post-fault control time stages as identified in [17]. This generic VSC model can vary the following time stages (from [17]): (i) fault inception period, during which the VSC has not yet responded to the fault condition and (ii) transition period, when the VSC starts its FRT control strategy. This model allows to control post-fault VSC dynamics of the I_q-injection by three parameters. The time delay t_d determines the fault inception period between fault incident and initiation of I_q-injection, i.e. when the VSC has no active response to the fault (Fig. 1b). Injection factor k determines the magnitude of the I_q-injection as function of the voltage drop (Fig. 1a). And r is the ramp rate at which I_q increases subsequently (Fig. 1b).

III. Methodology

This section first discusses the protection algorithms, studied network and lab setup for the protection tests. Then, preliminary results and the two case studies are discussed, namely the impact of underground cables and a VSC converter.

A. IQ protection algorithms in this study

This study focuses on directional algorithms to analyse the effects of changed source conditions on IQ protection. IQ distance algorithms start from the same fundamentals and can be seen as an extension of directional algorithms.

Two algorithms were selected because of their present application in commercial relays. Algorithm 1 from [9] is used in the described lab setup. Algorithm 1 is selected because the outputs of the different protection algorithms can be obtained separately. Algorithm 2 from [4] was implemented in EMT-type software and is used for pre-selection of cases via simulations. The process steps are identified below for both directional algorithms. This decomposition allows to analyse the similarities of both algorithms. This study focuses on the results from lab tests with hardware (section IV).

1) Process steps for algorithm 1:

- Digital anti-aliasing filter to down-sample 1 MHz samples to 10 kHz. Then additional low-pass filtering up to circa 2 to 2.5 kHz.
- Compute incremental values: $\Delta u = u(t) - u(t - T)$, with cycle period T and p=1.
- Compute the loop replica current based on RL line circuit. Compute acting and threshold quantities, representing instantaneous incremental powers.
- Comparison of integrated operating quantity versus threshold quantity.

2) Process steps for algorithm 2:

- Anti-aliasing filter, sampling at 2.4 kHz.
- Compute incremental values: $\Delta u = u(t) - 2u(t - T) + u(t - 2T)$, with T the cycle period.
- Compute operating quantity, representing instantaneous incremental power. Threshold quantity equals zero.
- Polarity of integrated operating quantity.

It is important to note that algorithm 1 uses a replica current which is computed based on a RL line circuit. By contrast, algorithm 2 directly uses the incremental quantities.

B. Studied network

The studied network (Fig. 2) allows to test IQ algorithms because Thévenin equivalent sources on both line ends represent the external grid (ideal case for the IQ algorithms)

and infeed conditions are changed at the local bus, which provides unconventional source behaviour for IQ algorithms. The impact of two different infeed conditions on the line protection is studied by either connecting a VSC from an HVDC-link or parallel underground cables e.g. to connect a wind farm.

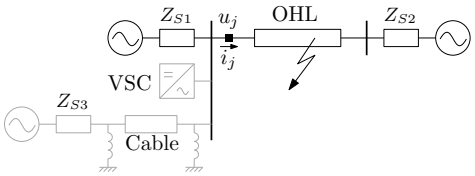

Fig. 2: Network modelled in PSCAD. Current and voltage waveforms are measured at the relay location (u_j and i_j).

The studied network topology resembles network conditions near the Belgian coast. It includes an overhead transmission line with at both line ends Thévenin equivalents representing the external grid. At one line end, either a set of 4 parallel underground cables with 50% shunt compensation at each side (case study I) or a VSC converter (case study II) is connected to the local, weaker bus. This system is modeled in EMT-type software [23]. The transmission line and underground cables are represented using the frequency dependent phase model. The Thévenin source models include both positive and zero sequence impedance of the external grid. A fault is applied at specific locations along the transmission line. Current and voltage waveforms measured at the relay location (u_j and i_j) are stored in COMTRADE format with a sample rate of 200 kHz, which is two orders of magnitude larger than the bandwidth of the filters used in IQ algorithms (III-A1).

All case studies make use of following parameters:

- The system phase-to-phase voltage is 400 kV.
- The line length is 100 km, with per unit length parameters evaluated at 50 Hz: r = 0.0332 Ω/km and x = 0.3264 Ω/km.
- The 4 parallel underground cables have a length of 12 km.
- The per unit length parameters for 1 cable evaluated at 50 Hz: r = 0.0123 Ω/km, x = 0.1982 Ω/km and c = 0.2214 μF/km.
- The converter has a rated power of 1000 MVA.
- The instrument transformers were assumed to be ideal, with ratios of 880 and 4000 for current and voltage, respectively.

The line geometry and material parameters of the overhead line and cables are provided in the Appendix (VI).

C. Lab setup

The setup, controlled by a python framework, allows to replay current and voltage waveforms generated with offline simulations on a physical protection device in the lab, in this case the SEL T400L protection relay. Figure 3 shows the different steps in the process. First, current and voltage waveforms are generated with PSCAD and stored in COMTRADE format for all combinations of a given parameter set. Then follows an automated replay of those waveforms using a real-time simulator [24] as signal generator. The digital signals are converted to analog low voltage inputs

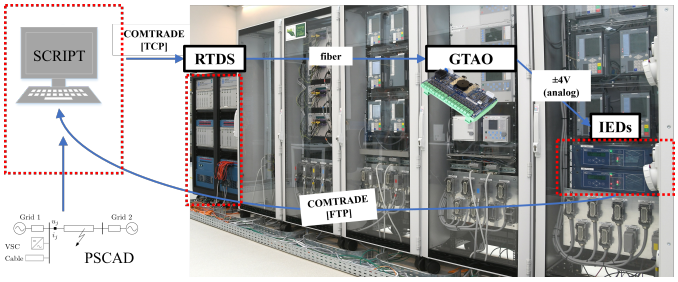

Fig. 3: Lab setup for automated replay of current and voltage waveforms from COMTRADE files.

and finally applied to the relay. The relay under test has an internal playback functionality without digital to analog signal conversion and can be automated as in [25], but it requires manual front panel acknowledgement which expires after one hour [9]. Therefore, automated testing was performed using a signal generator with sufficient bandwidth for testing IQ algorithms (section III-A1). The relay response to each event (digital outputs) is stored in event files and is obtained in COMTRADE format from the relay by File Transfer Protocol (FTP).

The relay settings are computed according to the recommendations in the manual. The forward impedance threshold is set to 30% of the system impedance assuming the strongest system conditions for each case study [9]. Similarly the reverse impedance threshold is set to 30% of the line impedance. The system impedance seen by the local bus is derived from the grid equivalents. The settings are computed per case study. For the case study with cables, the equivalent impedance includes source 1 in parallel with source 3 and the cables. For the case study with VSC, 1GVA of additional short-circuit power was taken into account at the local bus to compute the forward impedance setting.

D. Preliminary study

1) Network parameters and their effect on the resonance frequency:

Power system resonance frequencies induced by cables shift towards lower frequencies. This effect is driven by the non-negligible capacitance of cables, which is up to 20 times higher compared to overhead lines of the same length [1]. In the future, the resonance frequencies are expected to decrease more because of (i) increasing amount of cables installed in the system and (ii) the trend towards weaker systems driven by the renewable energy transition. As a result, these resonances can manifest within the bandwidth of the input filters of time-domain protection elements and potentially impede correct functioning of those elements.

The network parameters that affect the frequency and/or magnitude of the resonant oscillation were identified based on preliminary studies in Matlab and verification with PSCAD. This is done by a frequency scan of the equivalent impedance seen from the fault location for varying network parameters. Network and fault parameters were varied to analyse the sensitivity of the resonance frequency with respect to these parameters.

This preliminary study shows that the resonance frequency is most sensitive to the fault location (Fig. 4). Close faults lead to high resonance frequencies. Therefore smaller intervals were selected for close faults, and similar fine intervals for faults close to the remote line end. Grid strength has a smaller effect on the resonance frequency, but becomes more important in case of remote faults. The fault resistance only affects the magnitude of the peak of the equivalent impedance, not the resonance frequency.

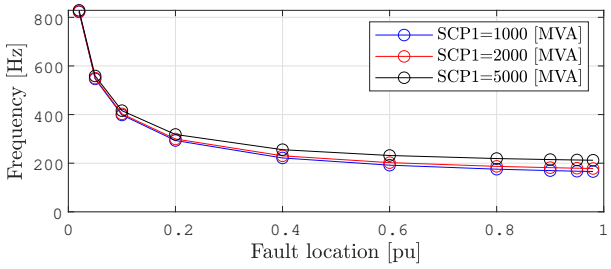

Fig. 4: Resonance frequency as function of fault location and grid strength of source 1.

The fault type affects the resonance frequency. Different fault types involve different sequence impedances. Three phase faults only involve the positive sequence. A single phase fault results in the series connection of the zero, positive and negative sequences (Z_{seq} in Fig. 5). This results in two valleys in Z_{seq}, with the first valley at a lower resonance frequency than for the positive sequence. Single phase faults therefore trigger lower resonance frequencies.

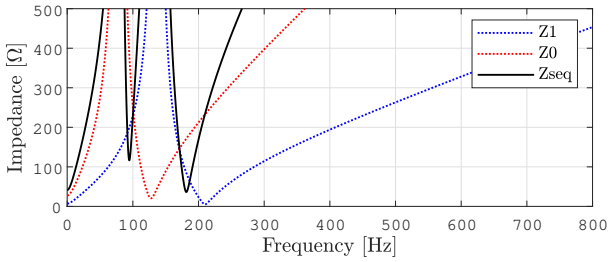

Fig. 5: Frequency scan of the positive, zero and loop impedance measured at the fault location. The valleys indicate series resonance [26]. This can be triggered by an excitation with a voltage source (e.g. a step change due to a fault).

2) Network parameters and their effect on VSC current phase shift:
During faults the injection angle depends on the implemented FRT control strategy [2]. The FRT strategy implemented in this study is explained in section II-B, and compared to a conventional synchronous source with an example in Fig. 6. The very large time delay in this example allows to visualise the transient control time-stages separately. The fault incident occurs at 55 ms, I_q-injection initiates at 105 ms after a 50 ms time delay. At the fault incident, the voltage shows oscillations caused by traveling wave reflections and limited damping in the test network with a fault close to the bus. These high frequency oscillations are filtered by the input filter of the IQ algorithm (III-A1).

During the fault inception period the VSC continues its active power control strategy. By contrast, the active power decreases due to the drop of voltage at the converter terminals

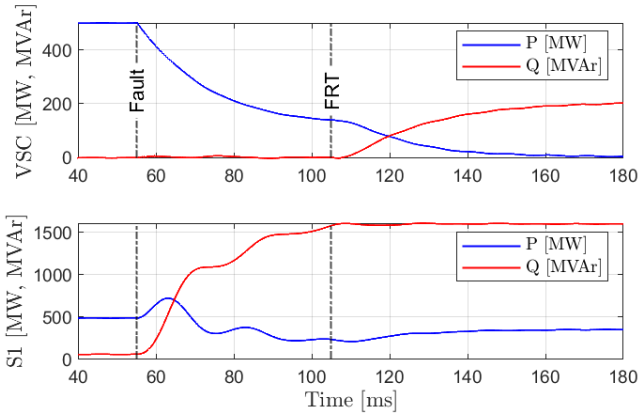

(a) Active and reactive power of VSC and source 1.

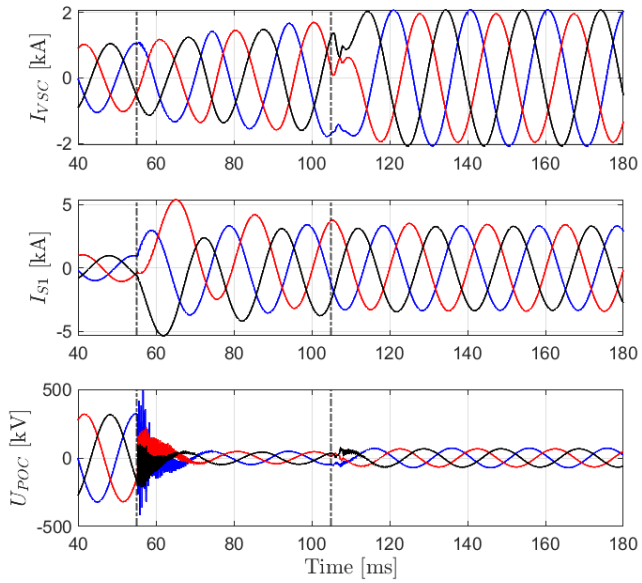

(b) Currents of VSC and source 1, and voltage at point of coupling.

Fig. 6: Comparison of VSC and synchronous generator time stages during fault. Fault inception period from 55 ms to 105 ms, and transition period from 105 ms onward with voltage support as FRT strategy with injection factor k=5 and high ramp rate (r=5000). The 50 ms time delay is exaggerated in this example for the purpose of visualisation. The power measurements are smoothed with a low-pass filter (20 ms time constant).

(Fig. 6). The current phase angle remains approximately constant. This differs from the synchronous generator. After the time delay (t_d exaggerated here) the VSC switches to the fault control strategy which aims to mimic the fault behaviour of a synchronous generator, which is in accordance with [27]. This mode switch introduces a phase jump. Unlike VSC the passive response of synchronous sources is determined by impedances in the sequence networks during fault. Therefore the fault response starts immediately at 55 ms and without a fault inception period as for the VSC.

The metrics to describe the phase angle shift are the magnitude and timing of that angle shift. Parameters that affect the timing of the phase shift are designed as such in the generic VSC model (II-B). The magnitude of angle shift is related to the ratio of (i) the reactive current injected by the VSC and (ii) current injected by conventional sources. The injected reactive current I_q by the VSC depends on the remaining voltage. The

angle shift magnitude consequently depends on parameters that determine the remaining voltage: fault resistance (R_f), fault location (x) and short circuit power of local and remote grids (SCP_1 and SCP_2). Second, the angle shift depends on the pre-fault angles of voltage and current.

E. In-depth study

1) Case study I: cable oscillations:

This case study analyses the impact of cable induced oscillations during faults on IQ protection. The parameter set for this case study is selected based on the preliminary studies discussed earlier. The following parameters are varied: fault location (FL), fault type (FT) and short circuit power of local grids (SCP_1 and SCP_3). Other parameters are kept constant. The forward $Z_{fwd,\ sec}$ = 1.09Ω and reverse $Z_{rev,\ sec}$ = 2.16Ω impedance settings are obtained as explained in III-C. The selected set of parameters (Table I) adds up to a total of: 10*2*3*3 = 180 cases. Finally this study loops over all parameter combinations to assess the response of the protection algorithm.

TABLE I: Parameter set for Case study 1

Parameter	Value
R_f	0 Ω
x	0.02, 0.05, 0.1, 0.2, 0.4, 0.6, 0.8, 0.9, 0.95, 0.98
FT	AG, ABCG
POW	90°
SCP_1	1000, 2000, 5000 MVA
SCP_2	10 000 MVA
SCP_3	1000, 2000, 5000 MVA

Zero fault resistance (R_f) is selected, and point on wave (POW) angle is at maximum voltage magnitude to cause a maximal voltage transient. The short circuit power of the remote source (SCP_2) does not affect the oscillation and is thus not varied, because a fault with zero resistance decouples both sides of the transmission line during fault. The pre-fault power flow is set to zero, because of its negligible effect compared to the parameters that were varied in this study.

2) Case study II: VSC converter:

This case study analyses the impact of changing injection angles, determined by VSC control, on IQ protection. A preliminary study analysed network parameters that affect the magnitude and timing of the angle shift.

TABLE II: Parameter set for Case study 2

Parameter	Value
R_f	5 Ω
x	0.4
FT	ABCG
POW	90°
SCP_1	1000, 2000, 3000, 4000, 5000 MVA
SCP_2	10 000 MVA
P	1000, 0, -1000 MW
k	0, 2, 5 A pu / V pu
t_d	0, 10 ms
r	5000 A pu /s

The short circuit power of the local bus (SCP_1) is selected to vary the angle shift based on the remaining fault voltage. The other parameters that affect remaining voltage are kept constant. A non-zero fault resistance is selected to allow sufficient remaining voltage during fault for the PLL. The VSC pre-fault power flow is varied between minimal and maximal active power. The effect of pre-fault reactive power injection by the VSC was not considered in this study. The ramp rate r is set sufficiently high and constant so that only the inner current control loops limit the rising time. This study considers only symmetric faults as explained in II-B. The forward $Z_{fwd,\ sec}$ = 1.76Ω and reverse $Z_{rev,\ sec}$ = 2.16Ω impedance settings are obtained as explained in III-C. The selected set of parameters (Table II) adds up to a total of: 5*3*3*2 = 90 cases. This case study loops over all parameter combinations to assess the response of the protection algorithm.

IV. Results and discussion

A. Case study I: cable

1) Cable resonance triggered at fault:

A low frequency oscillation is present in the voltages and currents for the cases with cable (Fig. 7a). This oscillation remains present in the incremental voltages and currents. The IQ waveforms show highly distorted IQs, which persist longer than one fundamental cycle period of 20 ms. By contrast, the benchmark without cables doesn't contain this oscillation, but a high frequency component with small amplitude (Fig. 7b). The latter is filtered out by the input filter of the relay and doesn't appear in the IQs. The IQ waveforms in the benchmark show expected behaviour: sinusoidal current in the faulted phase and three in-phase voltages.

2) Reverse bit asserted:

The digital outputs for the case with cable satisfy first the forward and then both forward and reverse conditions of the directional algorithm (Fig. 7a). The directional algorithm compares polarity of the incremental voltage and incremental replica current [9]. The expected polarity, which is based on RL models, is opposite for forward faults and same for reverse faults. However, due to the capacitive behaviour at the source, the oscillations induced in this case study affect the replica current and consequently this polarity relationship. In the benchmark case only the forward output is asserted, as expected.

Cable resonances shift to lower frequencies for remote, single phase faults under weak grid conditions. Therefore it is hard to remove this oscillation with extra low-pass filtering. This would require significant limitation on the bandwidth of the protection input filter, thus resulting in significantly slower protection algorithms (Fig. 8). In that case, there remains little added value with respect to traditional phasor-based protection.

In case study I with cables, the reverse output bit asserted in 41 of the 180 tested cases (Fig. 9), while not observed in the benchmark cases. For a forward fault, the desired output of a directional algorithm is the forward output bit only. This condition was satisfied for 60 benchmark cases without cables connected (SCP_3 not connected and SCP_1=2000, 3000 and 6000 MVA) for comparison with the cases in Table I. The reverse bit is problematic mostly for remote, single phase faults under weak grid conditions. For remote faults the cable resonances shift to lower frequencies (Fig. 4). In addition, resonance frequencies are lower for single phase faults compared to three phase faults, because the negative- and zero-sequence inductances are involved as well (Fig. 5).

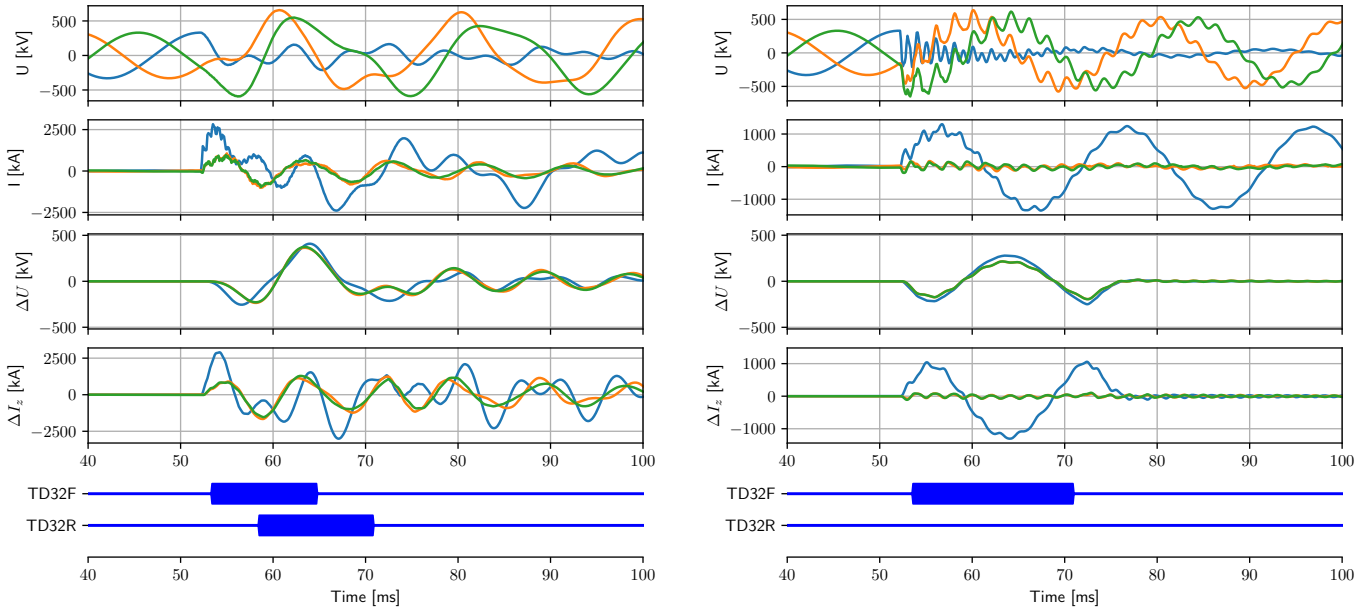

(a) Cable

(b) Benchmark

Fig. 7: Voltages and currents that are input to the relay and the digital outputs and IQ waveforms computed by the directional IQ algorithm, for a single phase fault (AG) located at 80% of the line length. The left shows an example case with underground cables (SCP_1=2000 MVA and SCP_3=1000 MVA behind cables) and a benchmark without cables (SCP_1=3000 MVA) at the right.

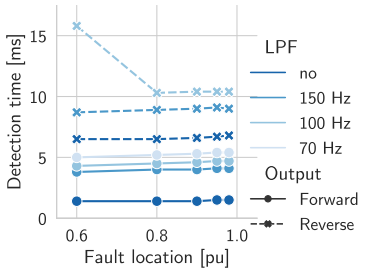

Fig. 8: Variation of the cutoff frequency of a low-pass filter and its impact on the forward and reverse detection. A third order low-pass Butterworth filter is added before the protection relay. 5 Fault cases are tested with SCP_1=SCP_3=2000 MVA which originally had both forward and reverse detection and an oscillation frequency between 180-200 Hz (with no extra filtering).

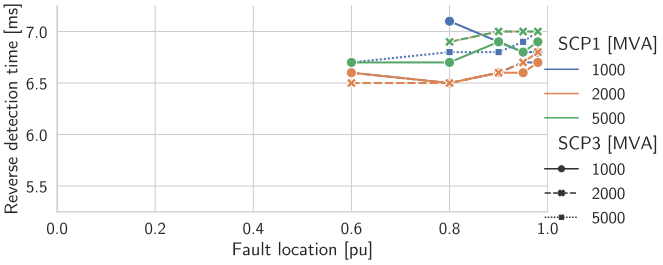

Fig. 9: Reverse detection time for single phase fault (AG) and varying short circuit powers of grids 1 and 3. Case study I.

3) Dependability decrease and potential security issues: Although the reverse bit is asserted in multiple cases, the forward bit is asserted first for all cases (Fig. 10). The time margin between the forward and reverse detection is around 5 ms for the cases in this study. This is a sufficiently large time margin compared to the expected operating time of 2 ms of the algorithm as reported in [6]. Therefore, no misoperations were observed in the test scenario's for this study. However, this study indicates a decreasing dependability margin, as the reverse detection condition is satisfied in 41 of the 180 tested cases. This is not observed in any of the benchmark cases.

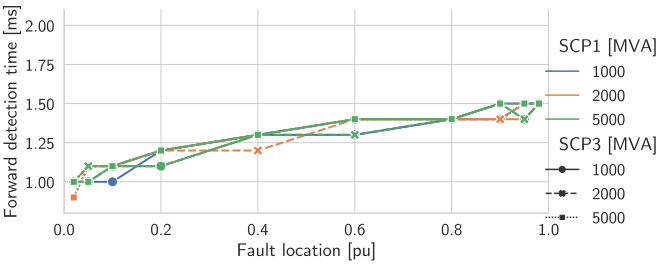

Fig. 10: Forward detection time for single phase fault (AG) and varying short circuit powers of grids 1 and 3. Case study I.

Additionally, security issues could arise for adjacent transmission lines. Cable oscillations change the expected polarity relationship of incremental voltage and replica current. As a result of polarity changes, the forward and reverse conditions are met successively (e.g. Fig. 7a). Analogously to the dependability tests in this study, reverse faults on adjacent lines could satisfy the forward condition leading to security issues. This requires further research.

B. Case study II: VSC converter

1) No forwards detection: In this case study with VSC, there was no forward detection in 6 of the 90 cases (Table II). On the other hand, the benchmark without the VSC correctly detects the forward faults. All of those undetected faults occurred in case of a weak synchronous source at bus 1 (SCP_1 = 1000 MVA) and zero pre-fault power flow of the VSC to the remote bus. Those undetected faults

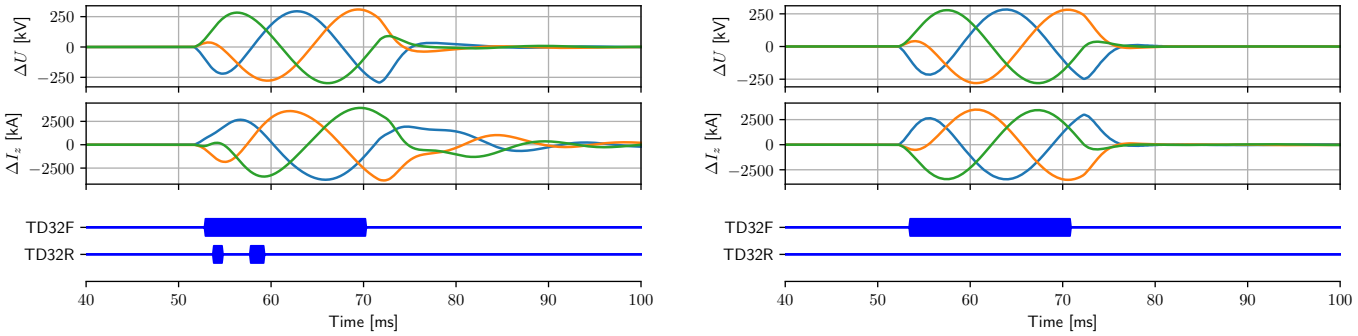

(a) VSC

(b) Benchmark

Fig. 11: Incremental voltages, replica currents and digital outputs computed by the relay for a three phase fault located at 40% of the line length. These values are derived from the relay. The left shows an example case with VSC and a benchmark without VSC at the right.

occurred independent from injection factor k. The cause of this can either be attributed to the small fault current contribution of the VSC, or the active power control during fault inception period which is different from synchronous behaviour.

2) Dependability problem and margin decrease: In 9 of the 90 tested cases (Table II), both the reverse and forward output bits are asserted. The angle shift by converter controls is visible in the IQ values during the first milliseconds after fault incident. Compare the current in Fig. 11a with the benchmark in Fig. 11b. The angle shift changes the replica current and consequently impacts the polarity relationship between the incremental voltage and incremental replica current (similar as explained in IV-A2). This results in the assertion of the reverse bit (e.g. Fig. 11a).

A VSC converter at bus 1 leads to a reduced time margin between the rise of the forward and reverse output bit (Fig. 12). In one case both the reverse and forward conditions are satisfied at the same instance. The fault direction consequently remains undecided. The time margin observed in this study decreases to values smaller than 1 ms and ranges from 0 to 1.25 ms. Network conditions that result in the smallest margin (Fig. 12) are: (i) fast initiation of I_q-injection after fault incident, (ii) weak grid connected to the local bus 1, (iii) positive or zero pre-fault power flow from VSC to the remote bus and (iv) I_q-injection with large injection factor k.

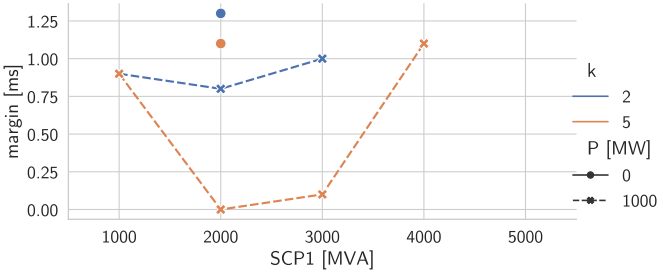

Fig. 12: Time margin between forwards and reverse detection for zero delay time (t_d=0 ms). Case study II.

The challenging network conditions for IQ protection identified here generally agree with the challenging conditions for conventional distance protection in the vicinity of VSC. The work in [15] identified challenges in case of a weak grid connected to the bus with VSC and observed a positive or negative effect of pre-fault power flow conditions.

V. Conclusions

Unconventional fault behaviour, that deviates from resistive-inductive behaviour, is not filtered out by the input filters of time-domain protection. Incremental quantity (IQ) protection does not extract the 50 Hz component as traditional phasor-based protection does. Application of time-domain protection such as IQ protection should therefore be handled with caution in future grids with VSC and/or increasing amount of underground cables. This work identified network parameters that affect cable resonant frequency and current phase shift by a VSC and their impact on IQ protection. This impact encompasses undetected faults, incorrect trip decisions and decreasing margins for a dependable trip decision.

Cables introduce low frequency oscillations, resulting in decrease of dependability margin and potential security issues. These oscillations change the expected polarity relationship of the IQ values calculated by the relay, which is explicitly or implicitly based on RL equivalent representation of the transmission grid. All 180 tested cases correctly identified the forward fault direction first, however, in 23% of the cases this was followed by a reverse detection after circa 5 ms. Cable resonances shift to lower frequencies for remote, single phase faults and additionally under weak grid conditions. To mitigate these effects, low-pass filtering should be applied, but this is detrimental to the speed of the algorithm.

Fast reactive current injection by a VSC can cause protection malfunction of IQ protection. The current injection introduces a phase shift during the first milliseconds after fault incident, which differs from passive RL behaviour and affects the expected polarity relationship of the IQ values. The vast majority of tested cases posed no problem, but attention should be paid for fast FRT controls and under low infeed circumstances, where the relative current contribution of the VSC is significant. In those cases, the results showed either incorrect behaviour or reduced dependability.

VI. Appendix

The overhead line (Table III) consists of 3 bundled conductors and a ground wire. The shunt conductance was set to 1.0E–11 S/m and the soil resistivity to 25 Ωm.

TABLE III: Overhead line geometry and material parameters

Parameter	**Conductors**	**Ground wire**
Radius	15.8 mm	11.2 mm
DC resistance	0.0635 Ω/km	0.278 Ω/km
μ_r	1	1
Coordinates (X, Y)	6.8, 54.4 m	4.2, 65.2 m
Coordinates (X, Y)	7.1, 43.4 m	
Coordinates (X, Y)	7.5, 32.4 m	
Sag	13.3 m	15.9 m
Bundled sub-conductors	2	
Bundle spacing	0.45 m	

The cable (Table IV) consists of a conductor, first insulation layer with semiconductor layers (2 and 1.3 mm for inner and outer layer, respectively), a sheath and outer insulation. The cable burial depth is 1.9 m for each phase, the shunt conductance was set to 1.0E–09 S/m and the soil resistivity to 25 Ωm.

TABLE IV: Cable geometry and material parameters

	Outer radius [mm]	ρ [Ωm]	ϵ_r [-]	μ_r [-]
Core	31.7	2.18E–08	1	1
Insulation	60.8		2.26	1
Sheath	61.1	1.72E–08	1	1
Insulation	65.9		2.26	1

References

[1] M. Bollen, S. Mousavi-Gargari, and S. Bahramirad, "Harmonic resonances due to transmission-system cables," in *The Renewable Energies and Power Quality Journal (RE&PQJ)*, no. 12, 2014.

[2] A. Hooshyar, M. A. Azzouz, and E. F. El-Saadany, "Distance Protection of Lines Emanating From Full-Scale Converter-Interfaced Renewable Energy Power Plants—Part I: Problem Statement," *IEEE Transactions on Power Delivery*, vol. 30, no. 4, pp. 1770–1780, Aug. 2015.

[3] E. O. Schweitzer, B. Kasztenny, A. Guzmán, V. Skendzic, and M. V. Mynam, "Speed of line protection - can we break free of phasor limitations?" in *2015 68th Annual Conference for Protective Relay Engineers*, College Station, TX, USA, 2015, pp. 448–461.

[4] GE Energy Connections Grid Solutions, *MiCOM P40 Agile, Technical Manual Numerical Distance Protection Relay*. GE Energy Connections Grid Solutions, P44x/EN M/Hb6.

[5] G. Benmouyal and J. Roberts, "Superimposed quantities: Their true nature and application in relays," in *Proceedings of the 26th annual western protective relay conference*, Spokane, Washington, USA, 1999.

[6] E. O. Schweitzer, B. Kasztenny, and M. V. Mynam, "Performance of time-domain line protection elements on real-world faults," in *2016 69th Annual Conference for Protective Relay Engineers (CPRE)*, College Station, TX, USA, 2016, pp. 1–17.

[7] P. Verrax, A. Bertinato, M. Kieffer, and B. Raison, "Fast fault identification in bipolar hvdc grids: A fault parameter estimation approach," *IEEE Transactions on Power Delivery*, vol. 37, no. 1, pp. 258–267, 2022.

[8] N. Johannesson and S. Norrga, "Longitudinal differential protection based on the universal line model," in *IECON 2015 - 41st Annual Conference of the IEEE Industrial Electronics Society*, Yokohama, Japan, 2015, pp. 1091–1096.

[9] Schweitzer Engineering Laboratories, *SEL-T400L Ultra-High-Speed Transmission Line Relay Traveling-Wave Fault Locator High-Resolution Event Recorder Instruction Manual*. Schweitzer Engineering Laboratories, 20190430.

[10] F. V. Lopes et al., "Time-domain relay performance evaluation considering brazilian fault cases," in *International Conference on Power Systems Transients (IPST2019)*, Perpignan, France, 2019, pp. 1–6.

[11] T. R. Honorato, V. R. Serpa, J. P. G. Ribeiro, E. A. Custódio, K. M. Silva, and F. V. Lopes, "On evaluating a time-domain distance element of a real relay for double-circuit transmission line protection," in *15th International Conference on Developments in Power System Protection (DPSP 2020)*, Liverpool, UK, 2020, pp. 1–6.

[12] B. Kasztenny, "Distance elements for line protection applications near unconventional sources," in *58th Annual Minnesota Power Systems Conference*, 2022.

[13] H. S. Samkari and B. K. Johnson, "Impact of distributed inverter-based resources on incremental quantities-based protection," in *2021 IEEE Power Energy Society General Meeting (PESGM)*, Washington, DC, USA, 2021, pp. 1–5.

[14] J. S. Costa et al., "Phasor-based and time-domain transmission line protection considering wind power integration," in *15th International Conference on Developments in Power System Protection (DPSP 2020)*, Liverpool, UK, 2020, pp. 1–6.

[15] W. Leterme, G. Chaffey, R. Loenders, J. Vermunicht, S. Shoushtari, and D. Van Hertem, "Systematic study of impedance locus of distance protection in the vicinity of vsc hvdc converters," in *16th International Conference on Developments in Power System Protection (DPSP 2022)*, Newcastle, UK, 2022, pp. 19–24.

[16] C. Brantl, P. Ruffing, and R. Puffer, "The application of line protection relays in high voltage ac transmission grids considering the capabilities and limitations of connected mmcs," in *15th International Conference on Developments in Power System Protection (DPSP 2020)*, Liverpool, UK, 2020, pp. 1–6.

[17] D. López et. al., "Negative sequence current injection by power electronics based generators and its impact on faulted phase selection algorithms of distance protection," in *Western Protective Relaying Conference (WPRC)*, Spokane, Washington, USA, Sep. 2018.

[18] J. Jia, G. Yang, A. H. Nielsen, and P. Roenne-Hansen, "Hardware-in-the-loop tests on distance protection considering vsc fault-ride-through control strategies," *The Journal of Engineering*, vol. 2018, no. 15, pp. 824–829, 2018.

[19] J. J. Chavez, M. Popov, A. Novikov, S. Azizi, and V. Terzija, "Protection function assessment of present relays for wind generator applications," in *International Conf. on Power Systems Transients (IPST2019)*, Perpignan, France, 2019, pp. 1–6.

[20] J. Wang, Y. Li, and F. Hohn, "Impact and challenges of conventional protection solutions in wind farm connected grids," in *16th International Conference on Developments in Power System Protection (DPSP 2022)*, Newcastle, UK, 2022, pp. 1–6.

[21] S. Beckler, H. Saad, and P. Rault, "On dynamic performance analysis for MMC-HVDC systems during AC faults," in *CIGRE Symposium Aalborg*, Aalborg, Denmark, 2019, pp. 1–11.

[22] S. Rüberg, et al., "Demonstration of mitigation measures and clarification of unclear grid code requirements," in *EU h2020 Migrate project*, no. Deliverable D1.6, 2019.

[23] Manitoba HVDC research centre, *User's Guide, on the use of PSCAD*. Manitoba, Canada, 2018.

[24] RTDS Technologies Inc., *RSCAD Fx instruction manual*. Winnipeg, Canada, 2022.

[25] T. R. Honorato, J. P. Ribeiro, E. A. Custódio, K. M. Silva, and F. V. Lopes, "Automated testing application for a novel playback functionality on a real time-domain relay," in *15th International Conference on Developments in Power System Protection (DPSP 2020)*, Liverpool, UK, 2020, pp. 1–6.

[26] CIGRE WG C4.307, "Resonance and ferroresonance in power networks." Technical Brochure TB 569, 2013.

[27] G. Ebner, B. Karacay, R. T. Pinto, E. Starschich *et al.*, "Enhanced voltage support with vsc-hvdc during unbalanced ac faults," in *CIGRÉ SC A3, B4 & D1 Colloquium*, Winnipeg, Canada, 2017, pp. 1–9.